Copper removal from semiconductor CMP wastewater in the presence of nano-SiO_2 through biosorption

Xiaoyu Wang, Gude Buer, Wei Fan, Lei Gao and Mingxin Huo

ABSTRACT

Copper-bearing wastewater from chemical mechanical planarization (CMP) is a typical semiconductor development byproduct. How to effectively treat Cu^{2+} in the CMP wastewater is a great concern in the microchip manufacturing industry. In this study, we investigated the potential for the microbial removal of Cu^{2+} by a multiple heavy metal-resistant bacterium *Cupriavidus gilardii* CR3. The environmental factors, including pH, nano-SiO_2, ionic strengths, and initial concentrations of Cu^{2+}, and adsorption times on the bioremoval of Cu^{2+} in CMP wastewater were optimized. Under optimal condition, the maximum biosorption capacity for Cu^{2+} was 18.25 mg g^{-1} and the bioremoval rate was 95.2%. The Freundlich model is described well for the biosorption of Cu^{2+} in CMP wastewater in the presence of nano-SiO_2 ($R^2 = 0.99$). The biosorption process obeyed the pseudo-second-order kinetic equation ($R^2 > 0.99$). In the column experiment, the advection–dispersion–retention model fitted the breakthrough curve of all experiments well ($R^2 > 0.95$). The attachment coefficient in the sand matrix coated by CR3 biofilm was 2.24–2.80 times as that in clean sand. Overall, *C. gilardii* CR3 is a promising candidate to remove Cu^{2+} from CMP wastewater. Nano-SiO_2 in CMP wastewater did not inhibit the bioremoval of Cu^{2+} but showed a slight promotion effect instead.

Key words | batch and packed column, biosorption, chemical mechanical planarization, metal-resistant bacteria

Xiaoyu Wang
Gude Buer
Wei Fan (corresponding author)
Lei Gao
Mingxin Huo
Engineering Lab for Water Pollution Control and Resources and Key Laboratory of Wetland Ecology and Vegetation Restoration, National Environmental Protection,
Northeast Normal University,
Changchun 130117,
China
E-mail: *fanw100@nenu.edu.cn*

HIGHLIGHTS

- Heavy metal-resistant bacterium *Cupriavidus gilardii* CR3 can effectively remove Cu^{2+} from the CMP wastewater in the presence of nano-SiO_2.
- Nano-SiO_2 under the common concentration in CMP wastewater does not affect the bioremoval of Cu^{2+}.
- The Freundlich model is better for describing the biosorption of Cu^{2+} CMP wastewater in the presence of Nano-SiO_2 relative to the Langmuir model.

INTRODUCTION

Increasing demand for advanced semiconductor products or microchips contributes to economic development in nations around the globe; however, it is also associated with a series of environmental issues. A major environmental problem is the large volumes of wastewater containing complicated contaminant composites generated from semiconductor manufacturing. Chemical mechanical planarization/polishing (CMP) is a vital process in semiconductor

doi: 10.2166/wrd.2021.098

manufacturing for dielectrics and metal layer planarization. In CMP, a considerable quantity of chemicals and ultrawater is needed to remove the residues of nanoparticles and chemicals on the semiconductor devices and achieve dielectrics and metal layer planarization. Thus, the resulting CMP wastewater contains various contaminants, which accounts for 40% of the entire semiconductor production process wastewater (Lai & Lin 2004). Once treated appropriately, CMP wastewater can be reclaimed and pressures on water resources can be relieved in the semiconductor industry.

In CMP wastewater, cupric ions (Cu^{2+}) pose a great concern due to their persistent nature, accumulation tendency, and biological toxicity. Cu^{2+} in CMP wastewater originated from copper metallization, as well as the application of $CuSO_4$ as oxidizing agents during the CMP. The concentrations of Cu^{2+} in CMP wastewater generally are presented as parts per million although the concentration of Cu^{2+} fluctuates in different ranges, for example, 5–100 mg L^{-1} (Maketon 2007). The reported concentration of Cu^{2+} in CMP wastewater is much higher than the level of copper toxicity toward aquatic organisms at 5–10 parts per billion (ppb) (Chua *et al.* 1999). Accordingly, appropriate treatment of Cu^{2+} in CMP wastewater is necessary to meet the local discharge standards of pollutants for the semiconductor industry. In the districts of the developed semiconductor industry, the permissible range of Cu^{2+} is from 0.2 to 1.0 mg L^{-1} depending on the receiving waters.

Cu^{2+} in CMP wastewater is usually treated by the electrochemical method (Yang & Tsai 2008), ion exchange resin method (Maketon & Ogden 2009), and membrane filtration (Su *et al.* 2014). However, the high initial costs and additional chemicals hamper the application of physical–chemical methods. Alternatively, biosorption by growing cells can offer advantages for the removal of heavy metal ions at low concentrations (Malik 2004). In the case of Cu^{2+} treatment in CMP wastewater, biosorption of Cu^{2+} in CMP wastewater has been reported (Stanley & Ogden 2003; Mosier *et al.* 2015). Our previous study also investigated the characteristics of *C. gilardii* CR3 to treat Cu^{2+} in CMP wastewater (Yang *et al.* 2017). However, the synthesized CMP wastewater used in the previous studies focused on the bioremoval of Cu^{2+}. The CMP requires nanoparticles as abrasive particles, for example, nanoparticle SiO_2 (nano-SiO_2), which is the common nanoparticle in the CMP, usually ranging from 0.05 to 0.50 g L^{-1} (Yang & Tsai 2008). But the treatment of Cu^{2+} rarely varies based on the presence of nano-SiO_2 in CMP wastewater. Hence, it should be considered whether the nano-SiO_2 can affect the biosorption of Cu^{2+} when CMP wastewater is treated.

In this study, we investigated the bioremoval of Cu^{2+} by a copper-resistant bacterium *C. gilardii* CR3 in the presence of nano-SiO_2. In the batch adsorption system, the treatment conditions were optimized and the bioremoval mechanisms of Cu^{2+} were examined. Further, the transport and retention of Cu^{2+} was studied in a fixed-bed column packed with sand coated by strain CR3.

MATERIALS AND METHODS

Bacterium and synthetic wastewater

The bacterium *C. gilardii* CR3 used in this study was isolated in our previous study (Yang *et al.* 2017). The cryopreserved *C. gilardii* CR3 cells were inoculated into a 100 mL Luria–Bertani (LB) medium and cultured in a constant temperature shaker at 28 °C for 24 h. Then the resurrected bacterial cells in 1 mL were transferred into a new 100 mL LB media. The suspension was centrifuged at 10,000 r min^{-1} for 5 min to collect the living cells. The received cells by centrifugation were washed with phosphate-buffered saline three times and the resulting cell suspension was used for the batch and column experiments. The growth curve of the strain in the LB medium is shown in Supplementary Material, Figure S1.

To stimulate the real CMP wastewater containing Cu^{2+} (Cu-CMP wastewater), the synthetic Cu-CMP wastewater was prepared with $CuCl_2{\cdot}H_2O$, nano-SiO_2 (50 nm), and deionized water.

Batch experiments

The effects of pH and nano-SiO_2 concentration, ionic strength, initial concentrations of Cu^{2+}, and contact time on the biosorption of Cu^{2+} by *C. gilardii* CR3 were studied. The concentration of Cu^{2+} used in batch experiments was 0.3 mM Cu^{2+} except for the test of Cu^{2+} initial concentrations. First, the pH (4.0, 5.0, and 6.0) and the

concentration of nano-SiO_2 (0.1, 0.3, and 0.5) in CMP wastewater were optimized. Afterwards, the effects of ionic strength, initial concentrations of Cu^{2+}, and contact time on the biosorption of Cu^{2+} were conducted under the optimized conditions in the first step (pH = 5, nano-SiO_2 = 0.3 g L^{-1}). The ionic strength was measured at 0, 1.0, 1.5, 2.0, 2.5, 3.0, 4.0, and 5.0 mM with a $NaNO_3$ solution. The initial Cu^{2+} concentration was set to 10 levels, from 0.1 to 1 mM with intervals of 0.1. The contact times on Cu^{2+} biosorption were conducted from 0 to 180 min at 28 °C. In control experiments, the aqueous Cu^{2+} was replaced with the same volume of deionized water. The removal rate and biosorption capacity of strain CR3 on Cu^{2+} were calculated according to the following formula:

$$q_e = \frac{v(C_0 - C_e)}{m} \tag{1}$$

$$\text{Removal rate } (\%) = \frac{C_0 - C_e}{C_0} \times 100 \tag{2}$$

where q_e is the biosorption capacity of Cu^{2+} by the unit of biosorbents in mg g^{-1}, C_0 and C_e are the initial and equilibrium concentration, respectively, of Cu^{2+} in the solution in mg L^{-1}, m is the mass of the biosorbents in g, and v is the volume of Cu-CMP wastewater in the system in L. In this study, Langmuir and Freundlich models were used to describe the equilibrium process of biosorption in batch experiments. The models are expressed as follows:

$$\frac{C_e}{q_e} = \frac{1}{q_m b} + \frac{C_e}{q_m} \tag{3}$$

$$\ln q_e = \ln K_F + \frac{1}{n} \ln C_e \tag{4}$$

in which q_e is represented as the biosorption capacity of Cu^{2+} by the unit of biosorbent in mg g^{-1}, C_e is the equilibrium concentration of Cu^{2+} in the solution in mg L^{-1}, q_m is the theoretical monolayer biosorption capacity in mg g^{-1}, n and K_F are the Freundlich equilibrium constants, and b is the Langmuir equilibrium constant.

To study the biosorption of the system, the experimental results are fitted with pseudo-first-order kinetics and pseudo-second-order kinetics. The first- and second-order equations are expressed as follows:

$$\log(q_e - q_t) = \log q_e - \frac{k_1}{2.303} t \tag{5}$$

$$\frac{t}{q_t} = \frac{1}{k q_e^2} + \frac{1}{q_e} t \tag{6}$$

where q_t and q_e, respectively, represent the biosorption time t and the amount of Cu^{2+} adsorbed by the biosorbent when they reach biosorption equilibrium in mg g^{-1} and k_1 and k_2 are the first and second rate equation constants.

Scanning electron microscope, Fourier-transform infrared spectroscopy, and zeta potential

A scanning electron microscope (SEM) (XL-30 ESEM FEG) was used to investigate the quartz sand, nano-SiO_2, and *C. gilardii* CR3 with Extracellular Polymeric Substances (EPS) in this study.

Quartz sand was ultrasonically cleaned three times and incubated with strain CR3 for 24 h. The quartz sand, strain CR3, and sand–strain CR3 were prepared into a 1.0 g L^{-1} suspension. The Zeta potential of strain CR3, quartz sand, and sand–strain CR3 was measured before and after the biosorption of Cu^{2+} using a Zeta potentiometer (Malvern Zetasizer Nano ZS90) under the pH 5.0, 0.3 mM Cu^{2+}, and 0.3 g L^{-1} nano-SiO_2 condition.

The sand–strain CR3 biosorbent samples before and after biosorption of Cu^{2+} were freeze-dried and ground with KBr at a ratio of 1:100. The sand–strain CR3 biosorbent samples were analyzed using Fourier-transform infrared (FTIR) spectroscopy (SHIMADZU FTIR-8400S).

Transport column experiments

The Cu^{2+} transport experiments were conducted using an acrylic column under saturated flow conditions (Supplementary Material, Figure S2). The column was 2.2 cm in inner diameter and 11 cm in effective length. Quartz sand with a diameter of 0.7–1.0 mm was packed in the column as a porous medium, and the packing density was 1.39 g cm^{-3}. Screens were installed at both ends of the column to prevent the packing from flowing out and distributing the flow

evenly. All column experiments were conducted in an upflow mode using a peristaltic pump (Lead Fluid BT102S) at a flow rate of 4 mL min^{-1}. All experiments were performed at room temperature (19.5 ± 1.2 °C).

The transport column experiments were performed with pulsed injection of Cu^{2+} solution, while Cu^{2+} solution was injected continuously in the latter. Both quartz sand and strain CR3-coated quartz sand was used as the packed medium in both sets of column experiments. Cu^{2+} solution and the mixture of Cu^{2+} and nano-SiO_2 solutions were used as two different input conditions to identify the role of nanoparticles during the process. The strain CR3-coated sand column was prepared according to the following procedure. The quartz sand (58 g) was sterilized by an autoclave at 121 °C for 30 min. Afterwards, the sterilized sand and the strain CR3 ($OD_{600} = 1.0$) were mixed in a 250 mL flask and were cultured for 24 h on a shaker (28 °C, 120 r min^{-1}). The cells of strain CR3 were attached to the sand surface. Then the composite of sand and strain CR3 was filled into the columns. Next, LB media was injected into the column for 12 h to multiply the bacteria followed by 12-h diluted LB (20%) elution and 2-h DI water elution. This elution process aimed to remove all dead bacteria in the column.

In this column experiment, 20 pore volumes (PVs) of the background electrolyte solution of interest were first passed through the column to ensure that the column was fully equilibrated with this solution. Then a solution containing Cu^{2+} within the same background electrolyte composition was injected into the column for 3.3 PVs, followed by elution with background solution again. Before the Cu^{2+} transport experiments, the tracer (Br^-) breakthrough tests were performed to estimate the hydraulic dispersion coefficient. The concentration of the Br^- was monitored at 1.5 min intervals by ion chromatography (Metrohm, 881 Compact IC pro, Switzerland). Normalized effluent concentrations (C/C_0) were plotted against the number of PVs to obtain the breakthrough curves (BTCs).

Mathematical modeling for column experiments

The transport of Cu^{2+} within the saturated sand column was described by an advection–dispersion–retention (ADR) model considering dynamic blocking and depth-dependent straining. The governing equations can be written as:

$$\frac{\partial(nC)}{\partial t} + \rho\frac{\partial S}{\partial t} = nD\frac{\partial^2 C}{\partial \chi^2} - q\frac{\partial C}{\partial \chi} \tag{7}$$

$$\rho\frac{\partial S}{\partial t} = nk_{\text{att}}\psi C - k_{\text{det}}\rho S \tag{8}$$

$$\psi = 1 - \frac{S}{S_{\max}} \tag{9}$$

where n is the porosity; C is the concentration of effluent Cu^{2+}; ρ is the bulk density of the porous media; S is the solid phase concentration adsorbed on the quartz sand; q is the flow rate; k_{att} and k_{det} are the first-order attachment coefficient and detachment coefficient, respectively; and ψ is a dimensionless function to account for the combined process of Langmuirian dynamics blocking and depth-dependent straining (Bradford & Bettahar 2006). $S_{\max}$ is the maximum solid phase particle concentration. The trace (Br^-) experiments were conducted before the Cu^{2+} penetration experiments to estimate the hydraulic dispersion coefficient (D). The above ADR model was fitted with the penetration curve to obtain k_{att}, k_{det}, and $S_{\max}$ parameters. The Cu^{2+} mass of water was calculated by the integral penetration curve BTCs based on the known Cu^{2+} mass input, and then the total adsorption mass of Cu^{2+} in the sand column was calculated according to the mass balance.

Measurement of Cu^{2+}

The Cu^{2+} concentration was measured by flame atomic absorption spectrometry (Varian 220FS, USA). All experiments were conducted in triplicate in this study. The data are given as mean values and the 95% confidence interval around the average value is indicated by error bars.

RESULTS AND DISCUSSION

Batch experiments – effects of pH, nano-SiO_2, ionic strength, initial Cu^{2+} concentration, and contact time

The pH value of the aqueous solution is an essential parameter that could affect the metallic ions biosorption (Alavi *et al.*

2015). The effects of pH value and nano-SiO_2 concentrations on the biosorption of Cu^{2+} by *C. gilardii* CR3 are shown in Figure 1(a) and Supplementary Material, Figure S3. Under all tested conditions of nano-SiO_2 (0, 0.1, 0.3, and 0.5 g L^{-1}), the bioremoval of Cu^{2+} reached a maximum at pH value of 5.0 compared with the results at pH value of 4.0 and 6.0. Thus, the optimized pH was 5.0. Under the optimized pH, the removal rate of Cu^{2+} was 95.4, 95.2, and 94.8% corresponding to the concentration of nano-SiO_2 at 0.1, 0.3, and 0.5 g L^{-1}, respectively, which were all higher than that in the absence of nano-SiO_2 (93.8%). Likewise, biosorption capacity for Cu^{2+} also exhibited the highest value at pH of 5 than that at pH 4 and 6 under different concentrations of nano-SiO_2 (Supplementary Material, Table S1). It is reported that the concentration of nanoparticle in the CMP usually ranges from 0.05 to 0.5 g L^{-1}, but in most cases, the nano-SiO_2 concentrations are about 0.3 g L^{-1} (Yang & Tsai 2006). Although the biosorption of Cu^{2+} from CMP wastewater has been investigated in previous studies (Stanley & Ogden 2003; Mosier *et al.* 2015; Yang *et al.* 2017), the effects of the presence of nano-SiO_2 on the removal of Cu^{2+} are not considered. In this study, bioremoval of Cu^{2+} and biosorption capacity for Cu^{2+} varied from 93.8%, 17.94 mg g^{-1} (nano-SiO_2 = 0 g L^{-1}) to 95.2%, 18.25 mg g^{-1} (nano-SiO_2 = 0.3 g L^{-1}) under the optimized pH of 5, indicating that the presence of nano-SiO_2 at actual concentration in CMP wastewater did not inhibit the Cu^{2+} removal but showed a slight promotion effect instead. According to our knowledge, this is the first study to investigate the effect of nano-SiO_2 on the bioremoval of Cu^{2+} in CMP wastewater.

Ionic strength is also an important factor affecting biosorption. The effect of different ionic strength for the biosorption of Cu^{2+} is shown in Figure 1(b). With the increase in ionic strength, the removal rate of Cu^{2+} decreased and reached the lowest (94.4%) at Na^+ concentration of 2.5 mM. The increase in ionic strength in solution will enhance the binding capacity of bacteria to Cu^{2+} (Darnall *et al.* 1986; Schiewer & Wong 2000). The competition of Na^+ and Cu^{2+} in solution

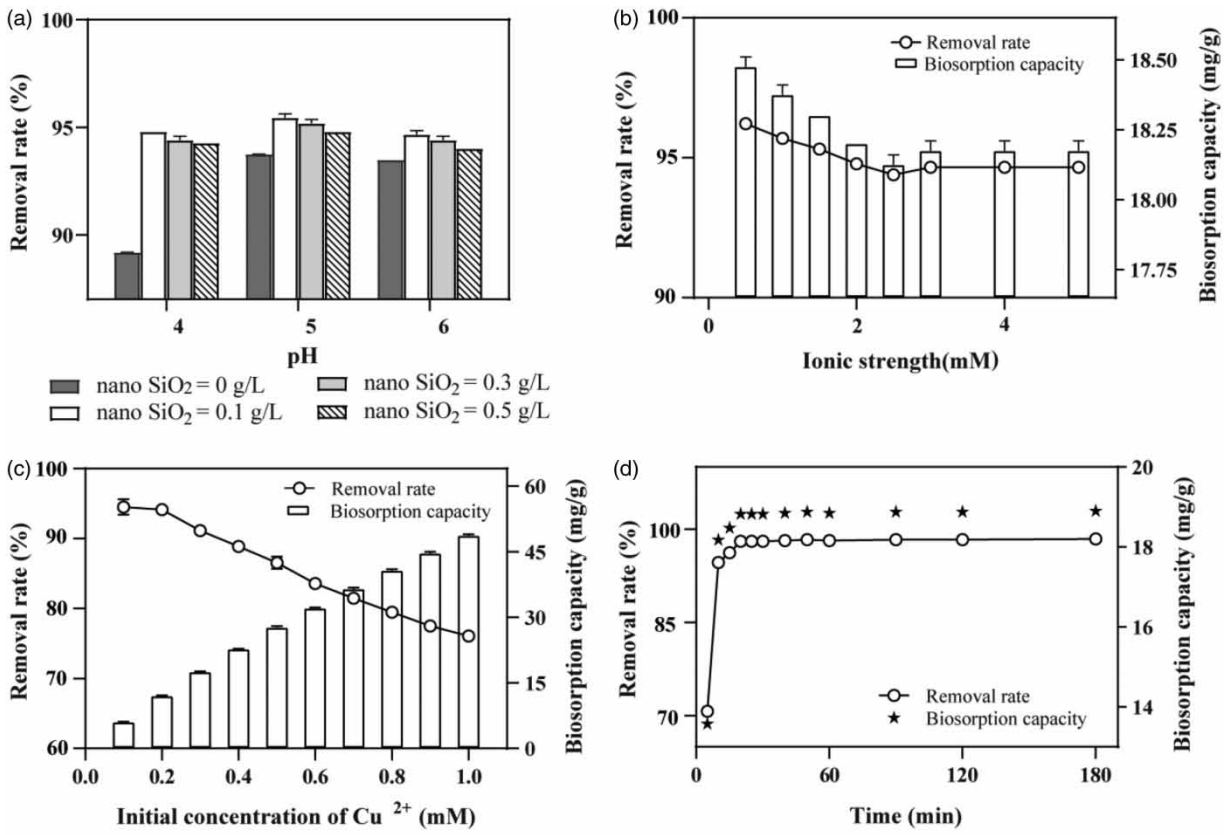

Figure 1 | Biosorption of Cu^{2+} by *C. gilardii* CR3 under static conditions: effect of pH and nano-SiO_2 (a), ionic strength (b), initial Cu^{2+} concentration (c), and contact time (d).

leading to Na^+ occupied a large number of biosorption sites on the surface of strain CR3. Hence, higher ionic strength decreased the bioremoval of Cu^{2+}.

The effect of the initial Cu^{2+} concentration on the bioremoval of Cu^{2+} by *C. gilardii* CR3 is shown in Figure 1(c). The removal rate of Cu^{2+} decreased with the increase in Cu^{2+} concentration (0.1–1.0 mM). The lowest removal rate of Cu^{2+} reached 91.2% at the common Cu^{2+} concentration (0.3 mM). When the Cu^{2+} concentration in CMP wastewater was 1 mM, the lowest removal rate of Cu^{2+} was still over 76.1% at 1 mM of Cu^{2+} concentration; the maximum biosorption capacity of Cu^{2+} was 48.7 mg g^{-1}. *Aureispira* sp. can remove approximately 90% of Cu^{2+} in a Cu^{2+} solution of 25–50 mg L^{-1} (Hasyimah *et al.* 2020). At the 1 mM concentration of Cu^{2+}, the maximum biosorption capacity of *Acidianus manzaensis* is 45.1 mmol kg^{-1} (Li *et al.* 2020). Hence, *C. gilardii* CR3 is a promising bacterial candidate for the treatment of Cu-CMP or other wastewater containing Cu^{2+} at a low concentration.

The effect of contact times for the biosorption of Cu^{2+} by the *C. gilardii* CR3 is shown in Figure 1(d). The removal rate of Cu^{2+} by the *C. gilardii* CR3 reached a maximum of 98% within the first 20 min. The removal rate of Cu^{2+} was almost stable from 20 to 180 min; the equilibrium biosorption capacity was 18.88 mg g^{-1}. It is known that the process includes two steps and the first step was rapid biosorption. First, a large number of biosorption sites on the surface of bacteria can be used to quickly adsorb Cu^{2+} (Liu *et al.* 2014). In the second step, biosorption equilibrium is reached and the biosorption sites are saturated, with the removal rate unchanged (Torab-Mostaedi *et al.* 2013). Our results were in agreement with this pattern.

Biosorption-isotherms and kinetics

Table 1 shows the results of relevant parameters using the Langmuir and Freundlich models. The Langmuir model fits well the related experimental data of Cu^{2+} initial concentration ($R^2 = 0.98$) (Supplementary Material, Figure S4). The predicted maximum biosorption capacity of *C. gilardii* CR3 was 59.62 mg g^{-1}, which was very close to the experimental biosorption capacity value (48.70 mg g^{-1}). For the Freundlich model, the fitting coefficient value is 0.99. In our previous study, the Langmuir model ($R^2 = 0.99$) was better than the Freundlich model ($R^2 = 0.49$) (Yang *et al.* 2017). Although Langmuir and Freundlich isotherms are usually used to simulate the biosorption in single ion solutions, they are slightly different. Specifically, the Langmuir model usually is used to describe the homogeneous monolayer biosorption, whereas the Freundlich model is used to describe heterogeneous biosorption (Veit *et al.* 2005). Our results indicated that the Freundlich model is better for describing the biosorption of Cu^{2+} CMP wastewater in the presence of nano-SiO_2.

Biosorption kinetics can show the binding speed of metal ions on the surface of the biosorbent (Michalak *et al.* 2013). Kinetic model fitting helps us to understand the reaction pathway and biosorption reaction mechanism in depth (Ho & McKay 2000). The experimental results in Figure 1(d) are fitted with quasi-first-order kinetics and pseudo-second-order kinetics models. The fitting results are shown in Table 2.

The fitting results of quasi-first-order kinetics and pseudo-second-order kinetics model are shown in Table 2. The fitting result of the quasi-first-order kinetic model was poor ($R^2 = 0.53$), thus the resulting q_e value (0.271 mg g^{-1}) is lower than the value of equilibrium biosorption capacity (18.88 mg g^{-1}). The pseudo-second-order kinetic model obeyed the experimental data ($R^2 > 0.99$). Meanwhile, the q_e value obtained by the pseudo-second-order kinetic is 18.97 mg g^{-1}, which is in good agreement with the equilibrium biosorption capacity.

Table 1 | Adsorption isotherms of *C. gilardii* CR3 for Cu^{2+}

Model	Parameter value		Correlation coefficient (R^2)	R_L	Fitting equation
Langmuir	$q_m = 59.620$	$b = 0.218$	0.989	0.067	$q_e = \frac{12.9746C_e}{1 + 0.2176C_e}$
Freundlich	$n = 2.120$	$K_F = 13.476$	0.998		$q_e = 13.4757C_e^{0.4714}$

Table 2 | Adsorption kinetics of *C. gilardii* CR3 for Cu^{2+}

Model	K	R^2	q_e (mg g^{-1})	Fitting equation
Quasi-first-order kinetics	0.015	0.5300	0.271	$\ln(q_e - q_t) = -1.3054 - 0.0151t$
Pseudo-second-order kinetics	0.102	0.9999	18.970	$\frac{t}{q_t} = \frac{t}{18.97} + 0.0273$

Analysis of SEM, zeta potential, and FTIR

The SEM images of *C. gilardii* CR3 before and post Cu^{2+} binding are shown in Figure 2. Compared to the sample without Cu^{2+} (Figure 2(a)), a large number of irregularly drawn EPS was covered or wrapped on the surface of bacterial cells (Figure 2(b)). The genome of *C. gilardii* CR3 includes EPS genes and a T3SS system responsible for secreting EPS; Cu^{2+} can lead to significant up-regulation of 11 genes of T3SS in *C. gilardii* CR3 (Huang *et al.* 2019a, 2019b). Hence, it can be inferred that Cu^{2+} stimulates the secretion of EPS. EPS is known as possessing a great capability for binding various metal ions (Comte *et al.* 2008). Additionally, EPS is beneficial to protect growing cells to avoid the toxic effect of heavy metal ions (Iyer *et al.* 2005). In sum, the increased EPS improved the ability of the bacterium cell surface to bind to Cu^{2+}, which further increased the biosorption of Cu^{2+}. Here, we provide a confocal laser scanning microscopy image of the EPS produced by the strain *C. gilardii* CR3 in Supplementary Material, Figure S5. The presence of protein and polysaccharides in EPS was indicated by a multiple fluorescence staining method (Cui *et al.* 2019).

The Zeta potential of strain CR3, quartz sand, and the composite of quartz sand–strain CR3 were measured before and after the biosorption of Cu^{2+} (Table 3). Among the three sorbents, the potential value of composite of quartz sand–strain CR3 was the most negative (−55.4 mV), followed by strain CR3 (−22.5 mV) and quartz sand (−45.9 mV) before biosorption of Cu^{2+}, which indicated that composite biosorbent carried more negative charges than that of strain CR3 and quartz sand. Likewise, the potential value showed a similar trend with the before biosorption of Cu^{2+}. Zeta potential represents the surface charge of the biosorbent and reflects the electrochemical properties of the biosorbent surface (van der Mei & Busscher 2001). Thus, the results show that the composite of quartz sand–strain CR3 is favorable to bind more Cu^{2+} as compared to strain CR3 and quartz sand because the composite possesses a stronger biosorption capacity for Cu^{2+}.

The results of the FTIR analysis showed that the peak shape of the composite of quartz sand–strain CR3 remained unchanged before and after the biosorption of Cu^{2+} (Figure 3). In other words, Cu^{2+} did not destroy the structure of the composite. In the composite of quartz sand–strain CR3, the major sorption peaks were as follows: 3,491 cm^{-1} corresponding to –NH and –OH stretching; 2,921 cm^{-1} corresponding to $-CH_2$ symmetrical or asymmetrical stretching; 1,082 cm^{-1} corresponding to C–OH/C–O–C/C–C/P = O; and the remaining absorption peak corresponds to the SiO_2 peak position in quartz sand. The specific functional groups on the surface of

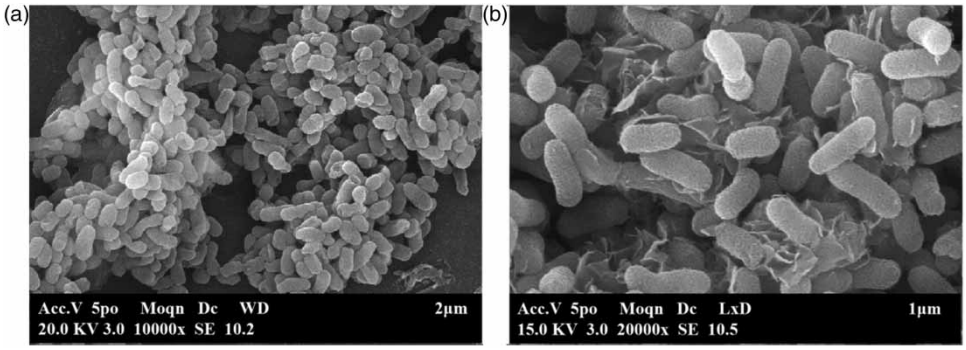

Figure 2 | SEM images of *C. gilardii* CR3 before (a) and after (b) Cu^{2+} binding.

Table 3 | Zeta potential of *C. gilardii* CR3, quartz sand, and the composite of quartz sand–strain CR3 before and after binding 0.3 mM Cu^{2+} at pH 5 and 0.3 g L^{-1} nano-SiO_2

	Zeta potential (mV)		
	Before biosorption	After biosorption	Absolute value
Strain CR3	−22.5	−18.5	4.0
Quartz sand	−45.9	−14.7	31.2
Sand–strain CR3	−55.4	−20.1	35.3

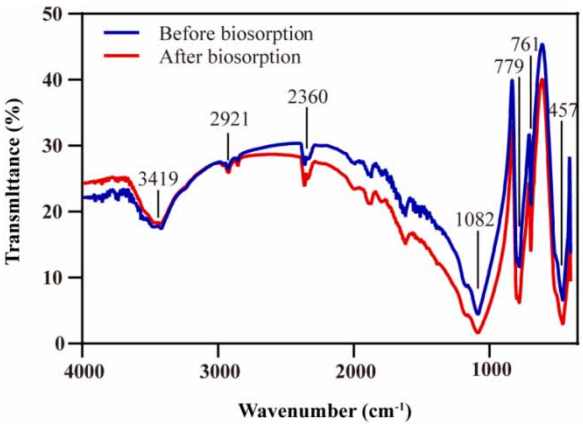

Figure 3 | The Fourier-transform infrared spectroscopy of the composite of quartz sand–strain CR3 before and after the biosorption of Cu^{2+} under the optimized condition (pH 5, 0.3 g L^{-1} nano-SiO_2).

the biosorbent play a key role in the biosorption of heavy metals (Bai & Abraham 2005). The main functional groups involved in the Cu^{2+} biosorption of the composite of quartz sand-strain CR3 were hydroxyl, carboxyl, amino, and phosphate groups, which played an important role in the binding with metal ions (Huang *et al.* 2013; Xia *et al.* 2015). The absorption peaks and shift indeed occurred before and after biosorption of Cu^{2+} although the variations of the absorption peaks were not obvious, which provided evidence that the composite of quartz sand–strain CR3 bound Cu^{2+} from the side of the functional groups on the sorbent.

Observed and modeled BTCs of the bioremoval of Cu^{2+} in columns

The observed and model-fitted BTCs of the tracer (Br^-) and Cu^{2+} in all columns are shown in Figure 4. The results of all tracer tests show very little difference with each other, and the maximum breakthrough concentrations, $(C/C_0)_{max}$, in all experiments were close to 1. This indicated good reproducibility of the experimental procedure (Fan *et al.* 2015). The hydrodynamic dispersion coefficient D was estimated as 0.28 ± 0.07 cm^2 min^{-1} ($R^2 > 0.96$). This fitted value of D was then used to model the transport of Cu^{2+}, and the best-fit transport parameters in the model are listed in Table 4 (the numerical model described all the experimental BTCs well, $R^2 > 0.90$). The mass percentages of Cu^{2+} recovered in the effluent, retained in the column, and total recovery ratio is summarized in Table 4. The recovery ratio ranges from 95.28 to 104.06%. The mass balance indicated that the operation and measurement were reliable.

As shown in Figure 4, the coexisting nano-SiO_2 could facilitate the transport of Cu^{2+}, since the retention ratio of Cu^{2+} was 29.73% in clean sand without nano-SiO_2 and it decreased to 23.90% when nano-SiO_2 was introduced. Nano-SiO_2 worked as the Cu^{2+}-carrier and promoted Cu^{2+} transport, which was further validated in the strain CR_3-coated column (Figure 4(b) and 4(c)). The presence of strain CR3 biofilm enhanced Cu^{2+} deposition both in the presence or absence of nano-SiO_2. The retention ratios of Cu^{2+} in strain CR3-coated sand columns (Figure 4(b) and 4(d)) were 1.24–1.37 times those in the clean sand columns (Figure 4(a) and 4(c)).

The variations of k_{det} and S_{max} in modeling verified these trends quantitatively. Higher values of k_{att} mean more intensive deposition of Cu^{2+} in the column. The k_{att} in the presence of nano-SiO_2 was only 0.174 of that in the absence of nano-SiO_2 in the clean sand columns, while this k_{att} was 0.565 in strain CR3-coated sand. After the sand was coated by the *C. gilardii* CR3 biofilm, the k_{att} increased 2.24–2.80 times the k_{att} in clean sand. The k_{det} was nearly 3–5 orders of magnitude lower than k_{att}, which confirmed that the remobilization of previously retained Cu^{2+} could be inconsiderable and the slight differences of k_{det} under these scenarios could be ignored. Overall, the presence of nano-SiO_2 could enhance Cu^{2+} transport and thus may increase spreading risk. By contrast, *C. gilardii* CR3 biofilm in the sand matrix can be a barrier to Cu^{2+} breakthrough.

The aforementioned facilitated bioremoval of Cu^{2+} by strain CR3 was confirmed by additional continuous flow column experiments, which was described in Section S1 in Supplementary Material. We employed two kinds of CMP

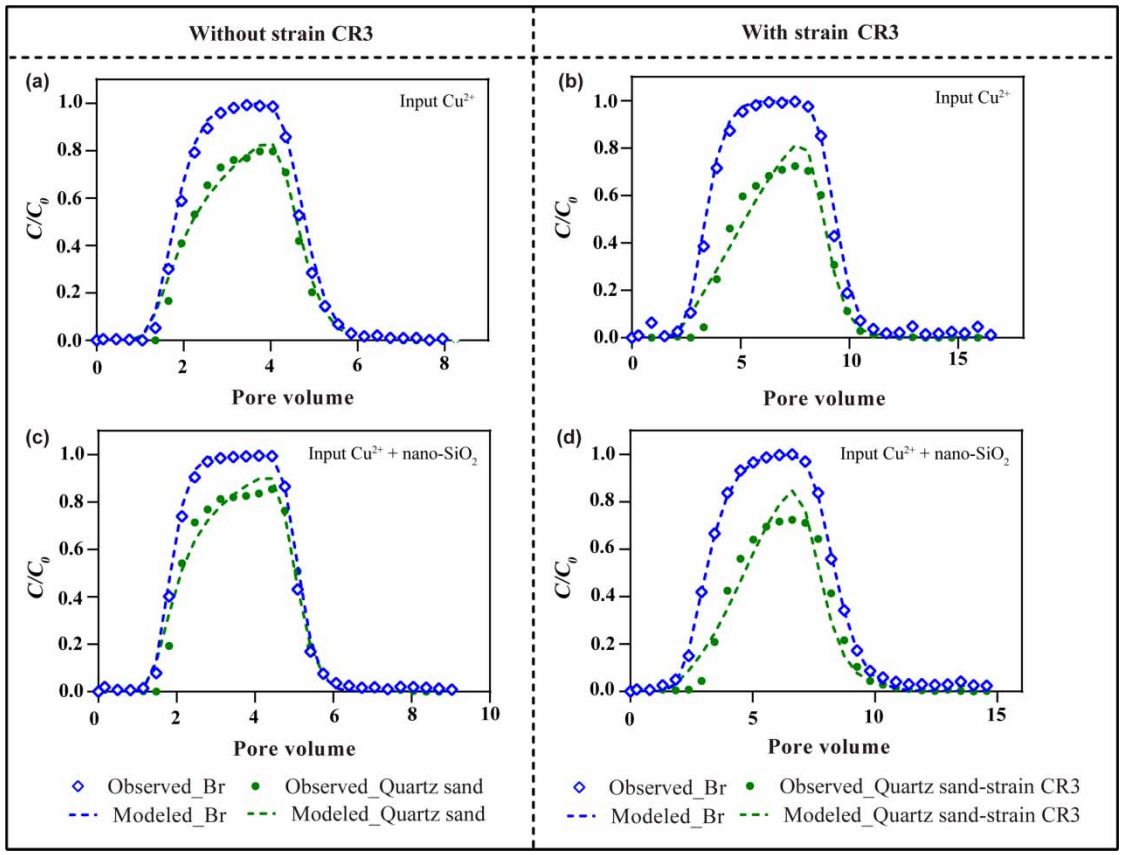

Figure 4 | Observed and modeled breakthrough curves of the tracer (Br^-) and Cu^{2+} in quartz sand columns under Cu^{2+} single solution control (a); Cu^{2+} single solution with strain CR3 (b); Cu^{2+} and nano-SiO_2 mixture solution control (c); Cu^{2+} and nano-SiO_2 mixture solution with strain CR3 (d).

Table 4 | Summary of experimental conditions and model results of Cu^{2+} transport

	Mass balance (%)							
Exp. no.	**Effluent**	**Retained**	**Total**	$(C/C_0)_{max}$	K_{att} (min^{-1})	K_{det} (min^{-1})	S_{max} (mg g^{-1})	R^2
a	72.19	29.73	101.92	0.8	0.215	0.001	0.176	0.987
b	59.10	37.13	96.23	0.72	0.818	0.001	0.256	0.967
c	80.16	23.90	104.06	0.85	0.174	0.004	0.132	0.984
d	62.50	32.78	95.28	0.72	0.565	0.005	0.259	0.957

wastewaters to be injected into the columns continuously: one only contained Cu^{2+} and one contained Cu^{2+} and nano-SiO_2 together. The results showed that the relative effluent concentration of Cu^{2+} (C/C_0) was higher in quartz sand without strain CR3 compared with that in CR3-coated sand matrix (Supplementary Material, Figure S6) for both of the two CMP wastewater, while the average C/C_0 at $t = 60$ min was 0.90 for the former and 0.81 for the latter. Note that the biosorption in these breakthrough columns was weaker than those in batch adsorption system; it can be attributed to the shorter hydraulic retention time in the columns (less than 12 min). Nevertheless, it still could be seen that the Cu^{2+} transportation was retarded by CR3 biofilm. By contrast, the differences between different C/C_0 curves in the same medium with/o nano-SiO_2 were less than 2.20% (Supplementary Material, Figure S6).

The coexistence of nano-SiO_2 did not inhibit this process, which was in keeping with the results of the batch adsorption experiments.

Overall, bacterial removal for heavy metal ions from wastewater is considered as an environmental friendly and cost-effective method, which is effective especially for ions at low concentrations. It is known that three mechanisms, including surface sorption, bioaccumulation, and biotransformation, are responsible for the bioremoval of metal ions (Li & Tao 2013). Among these, surface sorption occurring on the cell surface is the first step and metabolism-independent, and therefore accounts for a major part for heavy metal removal. The surface sorption of heavy metal ions depends on various factors, such as the nature of the bacterial species (the isoelectric point, the composition and structure of bacterial cell walls), heavy metal species, and pH value of the aqueous solution. According to the FTIR results and characteristics of bacterium *C. gilardii* CR3, we summarized the mechanisms of surface sorption Cu^{2+} in Figure 5. In the aqueous solution bearing copper, there are multiple ions, such as H^+, H_3O^+, OH^-, Cu^{2+}, and $Cu(OH)^+$. When the pH is lower to 2.2, i.e. the isoelectric point of strain CR3 (Yang *et al.* 2017), H^+, H_3O^+, and OH^- will compete the binding sites on the cell surface with Cu^{2+} and $Cu(OH)^+$, which means lower bioremoval of Cu^{2+}. If the pH value is over 5.0, some Cu^{2+} will present as $Cu(OH)_2$ according to the solubility product constant (2.2×10^{-20}). Since the aim of this study is to estimate the capability of bacterium to remove Cu^{2+}, higher pH condition (>5.0) is not considered although the insolubility of copper hydroxide can lead to small extra Cu^{2+} removal. When pH value ranges between 2.2 and 5.0, Cu^{2+} and $Cu(OH)^+$ are more preferable in the aqueous solution. As a result, these copper species will interact with the function groups (Figure 3), for example –SH, –OH, and –COOH, on the surface of microbial cells and increasing the binding of Cu^{2+}. In addition to the surface sorption, bioaccumulation and biotransformation also contribute to some extent to the removal of Cu^{2+}. Once the binding on the cell sites are fully occupied, bioaccumulation will contribute to the bioremoval of Cu^{2+} (Ayangbenro & Babalola 2017). At the same time, the intracellular Cu^{2+} might be effluxed out to keep the level of intracellular Cu^{2+} below the toxicity threshold (Machalová *et al.* 2015). It should be noted that the synthesized CMP wastewater used in the above-mentioned studies contained Cu^{2+} without nano-SiO_2. According to our knowledge, the finding in our study is the first to indicate that coexisting nano-SiO_2 does not inhibit the biosorption Cu^{2+} by strain CR3.

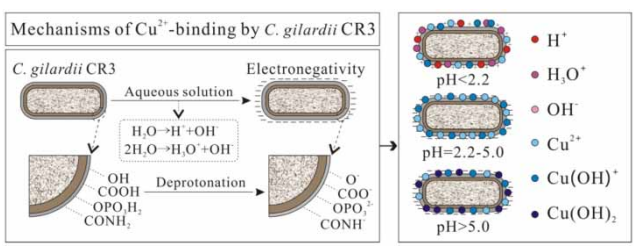

Figure 5 | Conceptual model for the Cu^{2+} binding onto the surface of *C. gilardii* CR3.

CONCLUSIONS

In this study, bioremoval of Cu^{2+} from CMP wastewater in the presence of nano-SiO_2 was investigated through batch adsorption experiments and transport column experiments using a typical copper-resistant bacterium *C. gilardii* CR3. The Freundlich isotherm is suitable for describing the biosorption process in Cu^{2+}-nano-SiO_2-CR3 ternary system. The biosorption kinetic data fit well with the pseudo-second-order equation. Overall, the maximum biosorption capacity for Cu^{2+} was 18.25 mg g^{-1} and the bioremoval rate was as high as 95.2%, displaying high removal efficacy of strain CR3. In the transport column experiments, the BTCs fit well with the ADR model. The attachment coefficient in the sand matrix coated by CR3 biofilm was 2.24–2.80 times as that in clean sand, confirming that CR3 biofilm can be a barrier to retard Cu^{2+} transport. In particular, in all experiments, the presence of nano-SiO_2 did not inhibit the bioremoval of Cu^{2+} from CMP wastewater but showed a slight promotion effect instead. Therefore, *C. gilardii* CR3 is a promising microbe biosorbent to remove Cu^{2+} from CMP wastewater even in the presence of nano-SiO_2.

ACKNOWLEDGEMENT

This work was funded by the National Natural Science Foundation of China (no. 51678122, no. 52070037, and no. 51978135).

DATA AVAILABILITY STATEMENT

All relevant data are included in the paper or its Supplementary Information.

REFERENCES

Alavi, S. A., Zilouei, H. & Asadinezhad, A. 2015 *Otostegia persica* biomass as a new biosorbent for the removal of lead from aqueous solutions. *International Journal of Environmental Science and Technology* **12** (2), 489–498. doi:10.1007/s13762-014-0705-x.

Ayangbenro, A. & Babalola, O. 2017 A new strategy for heavy metal polluted environments: a review of microbial biosorbents. *International Journal of Environmental Research and Public Health* **14** (1), 94. doi:10.3390/ijerph14010094.

Bai, S. R. & Abraham, T. E. 2005 Continuous adsorption and recovery of Cr(VI) in different types of reactors. *Biotechnology Progress* **21** (6), 1692–1699. doi:10.1021/bp050196c.

Bradford, S. A. & Bettahar, M. 2006 Concentration dependent transport of colloids in saturated porous media. *Journal of Contaminant Hydrology* **82** (1–2), 99–117. doi:10.1016/j.jconhyd.2005.09.006.

Chua, H., Yu, P., Sin, S. & Cheung, M. 1999 Sub-lethal effects of heavy metals on activated sludge microorganisms. *Chemosphere* **39** (15), 2681–2692. doi:10.1016/S0045-6535(99)00203-9.

Comte, S., Guibaud, G. & Baudu, M. 2008 Biosorption properties of extracellular polymeric substances (EPS) towards Cd, Cu and Pb for different pH values. *Journal of Hazardous Materials* **151** (1), 185–193. doi:10.1016/j.jhazmat.2007.05.070.

Cui, X., Chen, C., Liu, Y., Zhou, D. & Liu, M. 2019 Exogenous refractory protein enhances biofilm formation by altering the quorum sensing system: a potential hazard of soluble microbial proteins from WWTP effluent. *Science of the Total Environment* **667**, 384–389. doi:10.1016/j.scitotenv.2019.02.370.

Darnall, D. W., Greene, B., Henzl, M. T., Hosea, J. M., McPherson, R. A., Sneddon, J. & Alexander, M. D. 1986 Selective recovery of gold and other metal ions from an algal biomass. *Environmental Science & Technology* **20** (2), 206–208. doi:10.1021/es00144a018.

Fan, W., Jiang, X. H., Yang, W., Geng, Z., Huo, M. X., Liu, Z. M. & Zhou, H. 2015 Transport of graphene oxide in saturated porous media: effect of cation composition in mixed Na–Ca electrolyte systems. *Science of the Total Environment* **511**, 509–515. doi:10.1016/j.scitotenv.2014.12.099.

Hasyimah, N. A. R., Furusawa, G. & Amirul, A. A. 2020 Biosorption of a dye and heavy metals using dead cells of filamentous bacterium, *Aureispira* sp. CCB-QB1. *International Journal of Environmental Science and Technology* **18** (6), 1–10. doi:10.1007/s13762-020-02918-3.

Ho, Y. & McKay, G. 2000 The kinetics of sorption of divalent metal ions onto sphagnum moss peat. *Water Research* **34** (3), 735–742. doi:10.1016/S0043-1354(99)00232-8.

Huang, F., Dang, Z., Guo, C., Lu, G., Gu, R. R., Liu, H. & Zhang, H. 2013 Biosorption of Cd(II) by live and dead cells of *Bacillus cereus* RC-1 isolated from cadmium-contaminated soil. *Colloids and Surfaces B: Biointerfaces* **107**, 11–18. doi:10.1016/j.colsurfb.2013.01.062.

Huang, N., Mao, J., Hu, M., Wang, X. & Huo, M. 2019a Responses to copper stress in the metal-resistant bacterium *Cupriavidus gilardii* CR3: a whole-transcriptome analysis. *Journal of Basic Microbiology* **59** (5), 446–457. doi:10.1002/jobm.201800693.

Huang, N., Mao, J., Zhao, Y., Hu, M. & Wang, X. 2019b Multiple transcriptional mechanisms collectively mediate copper resistance in *Cupriavidus gilardii* CR3. *Environmental Science & Technology* **53** (8), 4609–4618. doi:10.1021/acs.est.8b06787.

Iyer, A., Mody, K. & Jha, B. 2005 Biosorption of heavy metals by a marine bacterium. *Marine Pollution Bulletin* **50** (3), 340–343. doi:10.1016/j.marpolbul.2004.11.012.

Lai, C. L. & Lin, S. H. 2004 Treatment of chemical mechanical polishing wastewater by electrocoagulation: system performances and sludge settling characteristics. *Chemosphere* **54** (3), 235–242. doi:10.1016/j.chemosphere.2003.08.014.

Li, P. & Tao, H. 2013 Cell surface engineering of microorganisms towards adsorption of heavy metals. *Critical Reviews in Microbiology* **41** (2), 140–149. doi:10.3109/1040841X.2013.813898.

Li, M., Huang, Y., Yang, Y., Wang, H., Hu, L., Zhong, H. & He, Z. 2020 Heavy metal ions removed from imitating acid mine drainages with a thermoacidophilic archaea: *Acidianus manzaensis* YN25. *Ecotoxicology and Environmental Safety* **190**, 110084. doi:10.1016/j.ecoenv.2019.110084.

Liu, Y., Cui, G., Luo, C., Zhang, L., Guo, Y. & Yan, S. 2014 Synthesis, characterization and application of amino-functionalized multi-walled carbon nanotubes for effective fast removal of methyl orange from aqueous solution. *RSC Advances* **4** (98), 55162–55172. doi:10.1039/C4RA10047F.

Machalová, L., Pipíška, M., Trajteľová, Z. & Horník, M. 2015 Comparison of Cd^{2+} biosorption and bioaccumulation by bacteria – a radiometric study. *Nova Biotechnologica et Chimica* **14** (2), 158–175. doi:10.1515/nbec-2015-0024.

Maketon, W. 2007 *Treatment of Cu-CMP Waste Streams Containing Copper(II) Using Polyethyleneimine (PEI)*. PhD Thesis. University of Arizona, Arizona, USA.

Maketon, W. & Ogden, K. 2009 Synergistic effects of citric acid and polyethyleneimine to remove copper from aqueous solutions. *Chemosphere* **75** (2), 206–211. doi:10.1016/j.chemosphere.2008.12.005.

Malik, A. 2004 Metal bioremediation through growing cells. *Environment International* **30** (2), 261–278. doi:10.1016/j.envint.2003.08.001.

Michalak, I., Chojnacka, K. & Witek-Krowiak, A. 2013 State of the art for the biosorption process – a review. *Applied Biochemistry and Biotechnology* **170** (6), 1389–1416. doi:10.1007/s12010-013-0269-0.

Mosier, A. P., Behnke, J., Jin, E. T. & Cady, N. C. 2015 Microbial biofilms for the removal of Cu^{2+} from CMP wastewater. *Journal of Environmental Management* **160**, 67–72. doi:10.1016/j.jenvman.2015.05.016.

Schiewer, S. & Wong, M. 2000 Ionic strength effects in biosorption of metals by marine algae. *Chemosphere* **41** (1–2), 271–282. doi:10.1016/S0045-6535(99)00421-X.

Stanley, L. C. & Ogden, K. L. 2003 Biosorption of copper (II) from chemical mechanical planarization wastewaters. *Journal of Environmental Management* **69** (3), 289–297. doi:10.1016/j.jenvman.2003.09.009.

Su, Y., Lin, W., Hou, C. & Den, W. 2014 Performance of integrated membrane filtration and electrodialysis processes for copper recovery from wafer polishing wastewater. *Journal of Water Process Engineering* **4**, 149–158. doi:10.1016/j.jwpe.2014.09.012.

Torab-Mostaedi, M., Asadollahzadeh, M., Hemmati, A. & Khosravi, A. 2013 Equilibrium, kinetic, and thermodynamic studies for biosorption of cadmium and nickel on grapefruit peel. *Journal of the Taiwan Institute of Chemical Engineers* **44** (2), 295–302. doi:10.1016/j.jtice.2012.11.001.

van der Mei, H. & Busscher, H. 2001 Electrophoretic mobility distributions of single-strain microbial populations. *Applied and Environmental Microbiology* **67** (2), 491–494. doi:10.1128/AEM.67.2.491-494.2001.

Veit, M. T., Tavares, C. R. G., Gomes-da-Costa, S. M. & Guedes, T. A. 2005 Adsorption isotherms of copper(II) for two species of dead fungi biomasses. *Process Biochemistry* **40** (10), 3303–3308. doi:10.1016/j.procbio.2005.03.029.

Xia, L., Xu, X., Zhu, W., Huang, Q. & Chen, W. 2015 A comparative study on the biosorption of Cd^{2+} onto *Paecilomyces lilacinus* XLA and *Mucoromycote* sp. XLC. *International Journal of Molecular Sciences* **16** (7), 15670–15687. doi:10.3390/ijms160715670.

Yang, G. C. C. & Tsai, C. 2006 Performance evaluation of a simultaneous electrocoagulation and electrofiltration module for the treatment of Cu-CMP and oxide-CMP wastewaters. *Journal of Membrane Science* **286** (1–2), 36–44. doi:10.1016/j.memsci.2006.09.007.

Yang, G. C. C. & Tsai, C. 2008 Preparation of carbon fibers/carbon/alumina tubular composite membranes and their applications in treating Cu-CMP wastewater by a novel electrochemical process. *Journal of Membrane Science* **321** (2), 232–239. doi:10.1016/j.memsci.2008.04.060.

Yang, Y., Hu, M., Zhou, D., Fan, W., Wang, X. & Huo, M. 2017 Bioremoval of Cu^{2+} from CMP wastewater by a novel copper-resistant bacterium *Cupriavidus gilardii* CR3: characteristics and mechanisms. *RSC Advances* **7** (30), 18793–18802. doi:10.1039/C7RA01163F.

First received 30 October 2020; accepted in revised form 23 December 2020. Available online 25 January 2021